ELSEVIER

Journal of Power Sources 79 (1999) 225–230

JOURNAL OF POWER SOURCES

Fabrication and characteristics of a composite cathode of sulfonated polyaniline and Ramsdellite–MnO_2 for a new rechargeable lithium polymer battery

K.S. Hwang *, C.W. Lee, T.H. Yoon, Y.S. Son

Department of Chemistry, Pukyong National University, 599-1 Daeyon 3-dong Nam-gu, Pusan 608-737, South Korea

Received 20 January 1999; accepted 27 January 1999

Abstract

The ionic conductivity of a polyacrylonitrile (PAN)-based solid polymer electrolyte is 1.4×10^{-3} S cm^{-1}, which is sufficient for the electrolyte to be used in a rechargeable lithium polymer battery. The anodic stability of the solid polymer electrolyte is over 4.6 V (vs. Li/Li^+). A reduced, highly sulfonated form of polyaniline (SPAn) and Ramsdellite–MnO_2 (R-MnO_2) are synthesized and used as a cathodic material for a rechargeable lithium polymer battery. Three kinds of cathodes are prepared from SPAn, R-MnO_2, and a mixture of SPAn and R-MnO_2. The electrochemical properties and diffusion coefficient of lithium ions in each cathode, and the interface between the solid polymer electrolyte and each cathode are investigated by cyclic voltammetry and impedance spectroscopy. The redox processes of the SPAn cathode are two-step reactions. The cathodic and anodic peak currents increase as the cycle number increases. In the redox processes of the R-MnO_2 cathode, the cathodic peak current on the second cycle is 62% of that on the first cycle. The $Li/$R-MnO_2 battery has a very high initial discharge capacity, but very poor cycleability. For the composite cathode, the cathodic peak current on the second cycle is 72% of that on the first cycle, i.e., higher than that for the R-MnO_2 cathode. The diffusion coefficient of the composite cathode during the discharge process is close to the sum of each variation in the SPAn and R-MnO_2 cathodes. The instability of the R-MnO_2 cathode at $x = 0.3$ and $x = 0.2$ during the charge process is not observed with the composite cathode. The discharge–charge performance of three types of battery are investigated. The initial discharge capacity of the Li/composite cathode battery is 97.0 m Ah g^{-1}. This battery has higher discharge capacity than the Li/SPAn battery (66.8 m Ah g^{-1}), and better cycleability than the $Li/$R-MnO_2 battery.

Keywords: Lithium polymer battery; Solid polymer electrolyte; Ramsdellite–MnO_2; Diffusion coefficient; Sulfonated polyaniline

1. Introduction

Polyaniline (PAn) is a promising conducting polymer for use in rechargeable lithium batteries due to its high conductivity, high theoretical specific capacity, and low cost. Because charge compensation in a Li/PAn battery is accomplished by large anions, however, a considerable amount of solvent is needed. PAn becomes insulating at pH ≥ 4 [1]. A reduced highly sulfonated form of polyaniline (SPAn) prepared by introducing $-SO_3H$ groups into the polyaniline chain, overcomes these disadvantages of the polyaniline. SPAn is a cation-exchanging conducting polymer and has relatively high ionic conductivity over a wide range of pH ≤ 7.5 and a good cycleability [2]. SPAn is also more stable that PAn [3].

Manganese dioxides are promising cathode materials because of their high specific energy, low toxicity, and low cost. Most of these materials have stable structures and good electrochemical lithiation properties [4]. The best known MnO_2 is comprised of γ-MnO_2 mixed with rutile–MnO_2 (β-MnO_2) and Ramsdellite–MnO_2 (R-MnO_2). The specific capacity of pure R-MnO_2 is high during initial discharge, but decreases rapidly with increasing cycle number [5].

In this paper, the properties of a polyacrylonitrile (PAN)-based solid polymer electrolyte (SPE) for a rechargeable lithium polymer battery are investigated. The electrochemical properties of SPAn, R-MnO_2 and a composite cathode material of SPAn and R-MnO_2 are evalu-

* Corresponding author. Fax: +82-51-6288147; E-mail: kshwang@dolphin.pknu.ac.kr

0378-7753/99/$ - see front matter
PII: S0378-7753(99)00157-3

ated by cyclic voltammetry. The impedance parameters of the SPE/cathode interface and the diffusion coefficient of lithium-ion insertion into the cathodes during the first discharge–charge process are determined by impedance spectroscopy. Finally, the discharge–charge performance of lithium batteries with three types of cathode are investigated.

2. Experimental

2.1. Active materials

2.1.1. Highly sulfonated polyaniline

Ammonium peroxydisulfate, $(NH_4)_2S_2O_8$, and aniline were dissolved in 1 M HCl. Emeraldine-based polyaniline was synthesized by means of the method reported by MacDiarmid et al. [6]. The emeraldine-based polyaniline was mixed with phenylhydrazine and became a more reduced form of polyaniline. The reaction product was sulfonated in fuming sulfuric acid to form the SPAn [2]. Characterization of the SPAn was carried out by means of FT-IR spectroscopy (Spectrum 2000, Perkin Elmer, USA). Elemental analysis of the SPAn showed a sulfur to nitrogen (S:N) ratio of ~ 0.63.

2.1.2. R-MnO_2

$LiMn_2O_4$ was synthesized by a solid-state reaction of 4 mol of MnO_2 and 1 mol of Li_2CO_3 in air at 450 and 700°C [7]. Pure R-MnO_2 was prepared by the digestion of spinel $LiMn_2O_4$ in 2.5 M H_2SO_4 at 95°C for 24 h [8]. The crystal structure was determined using a X-ray diffractometer (Rigaku, Japan) with Cu Kα radiation after three repeats of the drying and cooling processes.

2.2. Fabrication of cathodes

The cathodes were composed of active material, acetylene black and SPE binder at a composition of 35:10:55 by weight. Three kinds of active materials were used, namely, SPAN, R-MnO_2 and a mixture of 72 wt.% of SPAn and 28 wt.% of R-MnO_2. The composition (wt.%) of the SPE binder was 12.7 PAN: 44.8 EC: 42.5 PC. The SPE binder solution was heated at 110°C to obtain a sticky and transparent solution. A mixture of acetylene black and active material was prepared in a ball mill for 24 h and was added to the sticky solution to make a slurry. The slurry was pasted on a stainless-steel grid with a thickness of 100 to 500 μm, and then dried in argon-filled dry box [9].

2.3. Solid polymer electrolyte

The PAN-based polymer electrolyte was prepared according to the method of Abraham et al. [10]. The composition (mol.%) of the polymer electrolyte was 21 PAN: 40.15 EC: 32.85 PC: 6 $LiClO_4$. The ionic conductivity of the SPE was determined by a.c. impedance spectroscopy using a stainless-steel/SPE/stainless-steel blocking cell. The anodic stability of the SPE was also determined by sweep voltammetry using a Li/SPE/Li/SPE/stainless-steel cell. Lithium electrodes were used as reference and counter electrodes. A stainless-steel electrode served as the working electrode.

2.4. Investigation of electrochemical behaviour

The redox reactions of various cathodes were investigated by cyclic voltammetry. Lithium electrodes were used as reference and counter electrodes. Various cathodes served as the working electrode. The scan rate was 1 mV s^{-1}. The potential range in the case of the SPAn and the composite cathode (SPAn + R-MnO_2) was 2.5 to 4.4 V while that of the R-MnO_2 cathode was 1.2 to 4.4 V.

2.5. Impedance spectroscopy

Li/SPE/Li/SPE/cathode cells were fabricated using SPAn, R-MnO_2 and composite active-material. The first galvanostatic, intermittent, discharge–charge curves were obtained at a constant current density of 0.05 mA cm^{-2}. The impedance parameters of the SPE/cathode interface and the diffusion coefficient of lithium-ion insertion into the cathodes on the first discharge–charge process were determined by a.c. impedance spectroscopy. The impedance spectra were measured after the electrode attained an equilibrium potential. The potential after 20 min from the interruption of the current was considered to be the equilibrium potential. An a.c. potential of 10 mV was applied over the frequency range from 100 kHz to 0.01 Hz.

2.6. Discharge–charge performance

Rechargeable lithium polymer batteries were fabricated by sandwiching the polymer electrolyte laminate between a lithium foil anode and various cathodes. The sandwich was sealed in an aluminized polyethylene bag. The discharge–charge current density was 0.05 mA cm^{-2} and potential range was 2.5 to 4.4 V. The measurements were carried out with a battery test system (Albin, USA).

3. Results and discussion

3.1. Characteristics of solid polymer electrolyte

The equivalent circuit for describing the impedance of the blocking cell consists of a series circuit of resistance and capacitance. The electrolyte resistance was obtained from the intercept on the *x*-axis in Fig. 1. The ionic

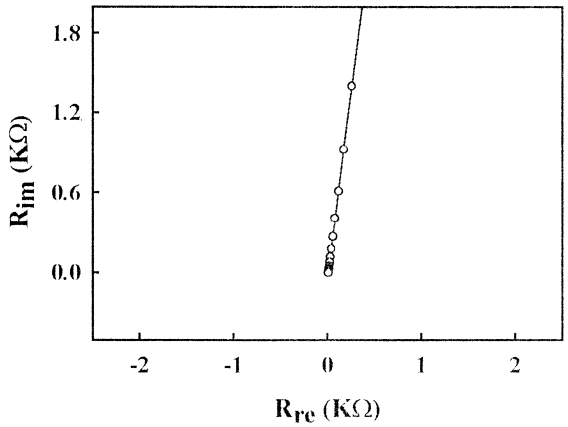

Fig. 1. Typical Nyquist plot of a stainless-steel/SPE/stainless-steel cell at room temperature.

conductivity was 1.4×10^{-3} S cm^{-1} at room temperature. This value indicates that application in a battery is feasible. A sweep voltammogram representing the anodic stability is shown in Fig. 2. The anodic stability of all the SPEs used in this work was as high as 4.6 V.

3.2. Electrochemical behaviour of various cathodes

Cyclic voltammograms for SPAn, R-MnO_2 and composite (SPAn + R-MnO_2) cathodes are shown in Fig. 3. The SPAn cathode displays two-step reactions in the redox processes and the peak current gradually increases with cycling (see Fig. 3a). This result suggests that a SPAn cathode can exhibit good cycleability in a battery application. The cathodic peak current of the R-MnO_2 cathode (Fig. 3b) decreases with cycling. For example, the cathodic peak current on the second cycle is 62% of that on the first cycle. This is due to destabilization of the R-MnO_2 framework structure on lithiation and to a large expansion/contraction of the unit cell during the redox processes [11]. In the case of the composite cathode (Fig. 3c), the cathodic

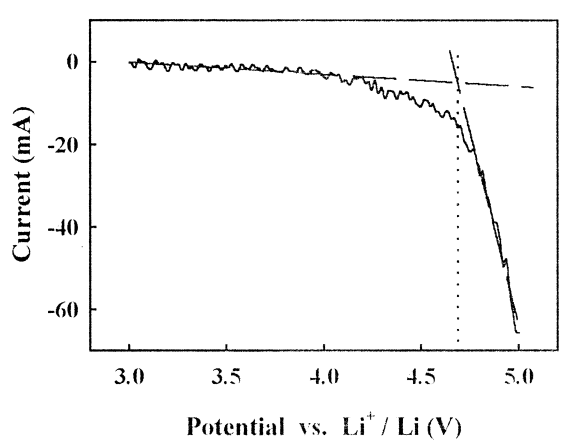

Fig. 2. Current–potential curve of a Li/SPE/stainless-steel cell at room temperature. Electrode area: 1.33 cm^2. Scan rate: 1 mV s^{-1}.

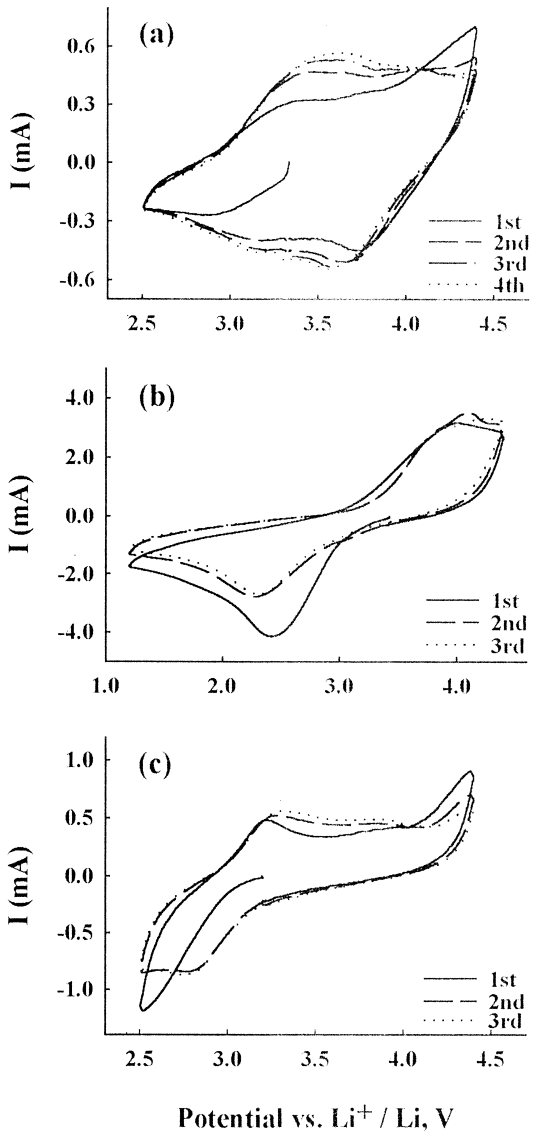

Fig. 3. Cyclic voltammograms of: (a) SPAn; (b) R-MnO_2; (c) composite cathode. Scan rate = 1 mV s^{-1}.

peak current on the second cycle is 72% of that on the first cycle. This value is higher than that in the R-MnO_2 cathode. This behaviour appears to result from the oxygen atoms in the SO_3^- group of the SPAn. The R-MnO_2 structure is transformed into a more stable structure, spinel $Li_2Mn_4O_9$, by heating in air [5].

3.3. Impedance parameters

Variations of the impedance parameters of the SPE/cathode interface on the first discharge–charge process were investigated. For these investigations, the equivalent circuit shown in Fig. 4 was assumed [12]. In this circuit, R_Ω is the electrolyte resistance, R_f is the film resistance of ClO_4^- oxidized on the cathode surface, R_{ct} is the charge-transfer resistance, and ω is the Warburg

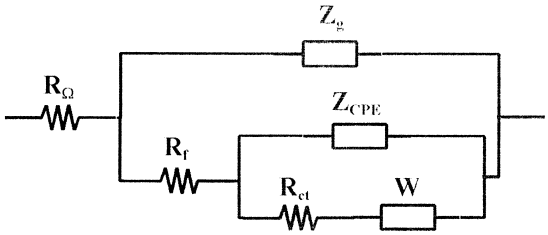

Fig. 4. Equivalent circuit of SPE/cathode interface.

impedance. Z_{CPE} is the impedance of the constant-phase element and is defined as [13]:

$$Z_{CPE} = A(j\omega)^{-\alpha},\ j = \sqrt{-1} \quad (1)$$

where ω is the angular frequency, A is a constant, and α is equal to $1-(2\theta/\pi)$. θ is the degree of clockwise rotation of the semi-circle in the impedance spectrum and is related to the inhomogeneity of the interface [14].

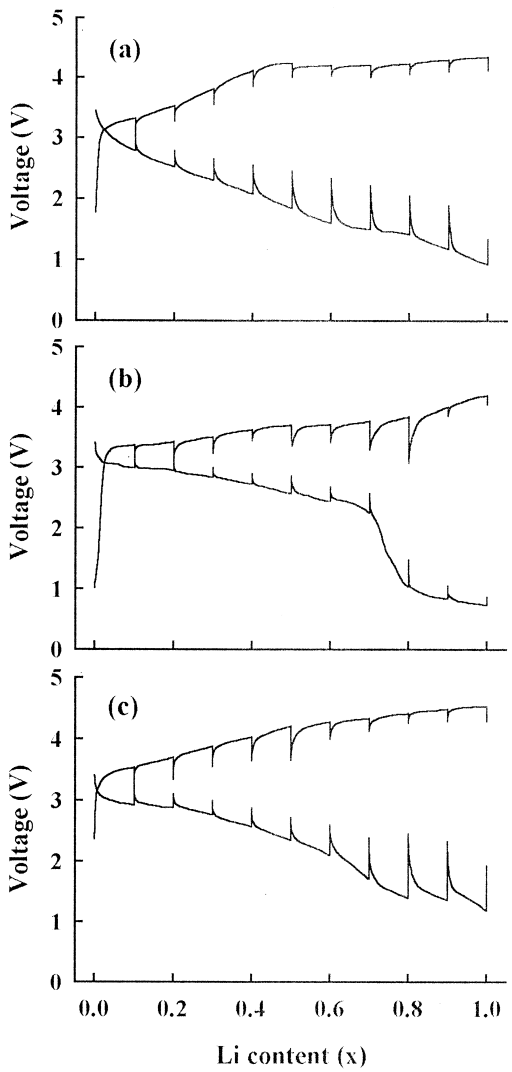

Fig. 5. First galvanostatic intermittent discharge–charge curves for cell of (a) Li/SPAn; (b) Li/R-MnO_2 and (c) Li/composite cathode. Current density of discharge–charge is 0.05 mA cm^{-2}.

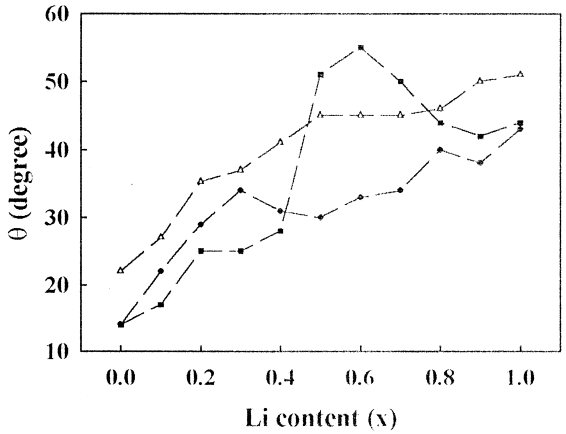

Fig. 6. Variation of θ value between SPE and various cathodes on lithium content (x) in cathodes during the first discharge process: (●) R-MnO_2; (■) SPAn; (△) composite cathode.

The first galvanostatic intermittent discharge–charge curves for the various cells are shown in Fig. 5. The impedance spectroscopy was performed with different lithium ion contents in the cathode. The variation of θ in the R-MnO_2 cathode in the first discharge process in Fig. 6 is similar to the transformation process of the R-MnO_2 structure on lithiation, i.e., a three-step reaction [5]. The θ increases rapidly up to $x = 0.3$ and is then constant between $x = 0.3$ and $x = 0.7$. After $x = 0.7$, θ increases again. In the case of the SPAn cathode, the θ increases rapidly up to $x = 0.6$, then decreases. The inhomogeneity at the SPE/SPAn interface on the insertion of lithium ions into the SPAn cathode causes the increment in θ. The decrease of θ is possibly caused by the start of non-polarization at $x = 0.6$ in Fig. 5(a). The variation of θ in the composite cathode is similar to the sum of each variation in the SPAn and the R-MnO_2 cathode.

The variation in θ in the various cathodes on the first charge process is shown in Fig. 7. The θ of the R-MnO_2

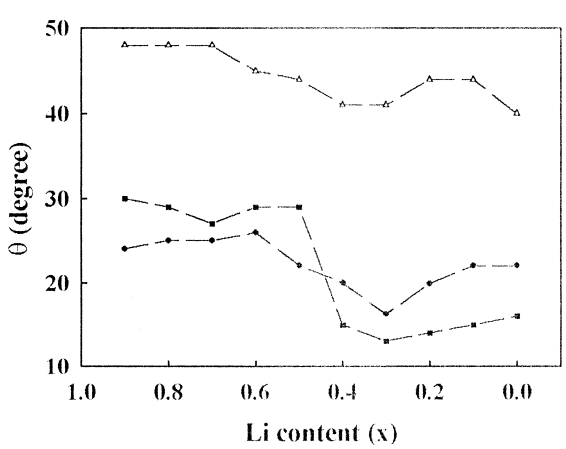

Fig. 7. Variation of θ between SPE and various cathodes on lithium content (x) in the cathodes during the first charge process: (●) R-MnO_2; (■) SPAn; (△) composite cathode.

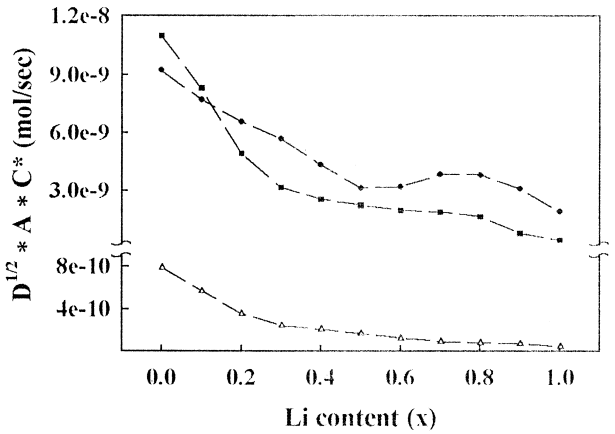

Fig. 8. Dependence of diffusion coefficient in various cathodes on lithium content (x) in the cathodes during the first discharge process: (●) R-MnO_2; (■) SPAn; (△) composite cathode.

cathode is maintained during the initial charge and decreases from $x = 0.6$ to $x = 0.3$, then increases after $x = 0.3$. This variation appears to be related to the transformation process of the R-MnO_2 structure, like that on the first discharge. Oxidation of SPAn proceeds via a two-step reaction (Fig. 3(a)). After equilibrium of the cathode with the electrolyte, charge compensation at each step is achieved by lithium ions. On the first charge process (i.e., before the equilibrium), however, charge compensations on the first and second steps are achieved by lithium ions and ClO_4^- ions, respectively [15]. During the initial charge, θ is constant. This is possibly results from the offset in the decrement factor by the increment factor. The increment factor is due to the film layer formed on the cathode surface by the anion on the initial charge. The decrement factor is the egress of lithium ions from the cathode. The sudden decrease of θ at $x = 0.6$ suggests that the ingress of ClO_4^- ions produces the film layer on the cathode surface, i.e., the second oxidation step commences. The variation of θ in the composite cathode appears to be affected by R-MnO_2 and SPAn cathodes. The θ decreases from $x = 0.3$ to end of charge.

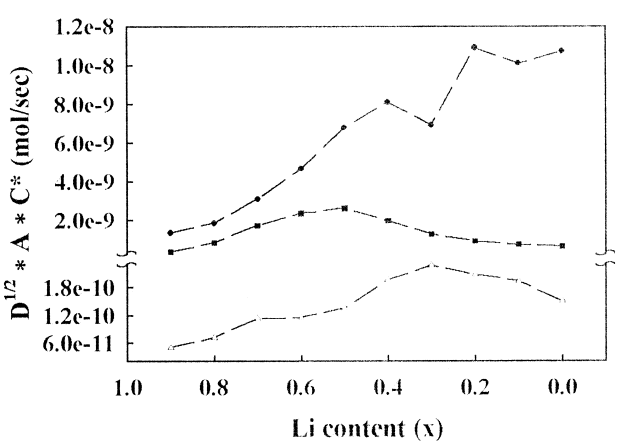

Fig. 9. Dependence of diffusion coefficient in various cathodes on lithium content (x) in the cathodes during the first charge process: (●) R-MnO_2; (■) SPAn; (△) composite cathode.

3.4. Diffusion coefficient

The Warburg coefficient (σ) was obtained from the slope of the straight line in the Randle's plot (Z_{re} vs. $\omega^{-1/2}$). The diffusion coefficients were calculated from [16]:

$$\sigma = \frac{RT}{n^2F^2A\sqrt{2}}\left(\frac{1}{D^{1/2}C^*}\right) \quad (2)$$

where D is the diffusion coefficient; C^* is the bulk concentration of the active material; and A is the electrode area.

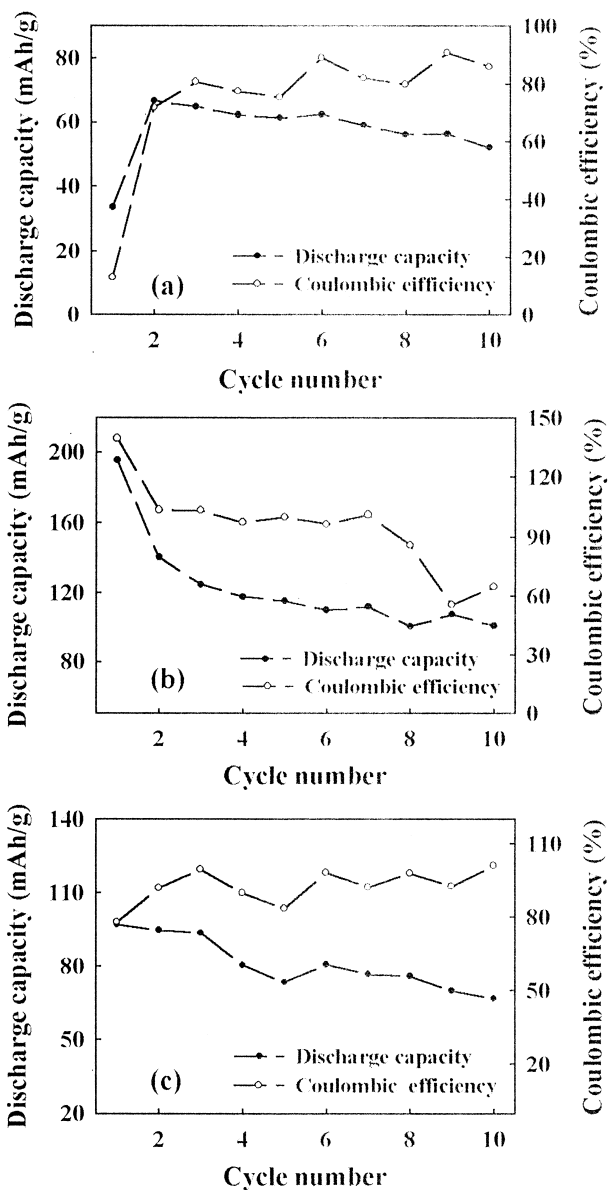

Fig. 10. Discharge capacity and coulombic efficiency as a function of cycle number for (a) Li/SPAn, (b) Li/R-MnO_2 and (c) Li/composite cathode batteries.

The variation of the diffusion coefficient in the various cathodes on the first discharge are shown in Fig. 8. The diffusion coefficient decreases with increasing lithium content in the cathode on initial discharge. If all sites have an equal probability of being occupied by lithium ions, the diffusion coefficient is proportional to the fractional number of vacant sites [12]. Therefore, because of the decrease in the fractional number of vacant sites, the diffusion coefficient is decreased. The activation energy for a lithium ion to jump from one site to the next is proportional to the coulombic attraction force between the lithium ion and the oxide lattice [12]. The coulombic attraction force is affected by a slight change in the lattice constant. Thus, the constant diffusion coefficient between $x = 0.4$ and $x = 0.9$ in the R-MnO_2 cathode is due to a decrease in the coulombic attraction force by transformation of the R-MnO_2 structure. The diffusion coefficient in the SPAn cathode is constant from $x = 0.5$ to $x = 0.6$. This range corresponds with that of the non-polarization of the SPAn cathode in the discharge curve in Fig. 5(a). The diffusion coefficient in the composite cathode decreases rapidly up to $x = 0.3$ and slowly after $x = 0.3$.

The diffusion coefficient in various cathodes on the first charge process is in the case of the SPAn cathode, the diffusion coefficient increases up to $x = 0.5$ (Fig. 9). This is because the fractional number of vacant sites increases as the lithium ions leave the SPAn cathode on the first oxidation step. On the second oxidation step, however, ClO_4^- ions enter the SPAn cathode, and the fractional number of vacant sites decreases. Therefore, the diffusion coefficient decreases after $x = 0.5$. The diffusion coefficient in the R-MnO_2 cathode increases as the lithium ions are extracted, but exhibits an unstable variation between $x = 0.3$ and $x = 0.2$. This is due to the unstable transformation of the R-MnO_2 structure. The variation of the diffusion coefficient in the composite cathode does not exhibit destabilization between $x = 0.3$ and $x = 0.2$ and is similar to that in the SPAn cathode.

3.5. Discharge–charge performance

The discharge capacity and the coulombic efficiency of batteries using the various cathodes are given in Fig. 10. The discharge capacity of the Li/SPAn battery on the 10th cycle is 78% that on the second cycle (66.8 m Ah g^{-1}). The second discharge capacity of the Li/R-MnO_2 battery is 72% of the first discharge capacity (195.4 m Ah g^{-1}) and the 6th discharge capacity is 78% of the second discharge capacity. 78% of the first discharge capacity (97.0 m Ah g^{-1}) of the Li/composite cathode battery is maintained until the 8th cycle. Thus, the Li/composite battery displays better cycleability than the Li/R-MnO_2 battery and a higher discharge capacity than the Li/SPAn battery. The coulombic efficiency of the Li/SPAn battery on the initial cycle is low but increases as the cycle number increases. This is because reduction of the SPAn on the first cycle is completed by only a one-step reaction [15]. The coulombic efficiency of the Li/R-MnO_2 battery suddenly decreases on the second cycle. This is because lithium ions inserted into the R-MnO_2 cathode on the first discharge are not extracted completely on the first charge due to the unstable transformation of R-MnO_2 structure.

4. Conclusions

The cathodic current of the composite cathode on the second cycle of the redox processes is 72% of that on the first cycle. This value is higher than that recorded for the R-MnO_2 cathode. This inhomogeneity of the SPE/composite cathode interface decreases after $x = 0.3$ on the first charge. This variation is not observed in either the R-MnO_2 or the SPAn cathode. From these results, it appears that the R-MnO_2 structure is stabilized by SPAn. The first discharge capacity (97.0 m Ah g^{-1}) of the Li/composite cathode battery is higher than that (66.8 m Ah g^{-1}) of the Li/SPAn battery, and its cycleability is better than that of the Li/R-MnO_2 battery.

References

[1] E.M. Genies, A. Boyle, M. Lapkowski, C. Tsintavis, Synthetic Metals 36 (1990) 139.
[2] X.L. Wei, Y.Z. Wang, S.M. Long, C. Bobeczko, A.J. Epstein, J. Am. Chem. Soc. 118 (1996) 2545.
[3] J. Yue, Z.H. Wang, K.R. Cromack, A.J. Epstein, A.G. MacDiarmid, J. Am. Chem. Soc. 113 (1991) 2665.
[4] G. Pistoia, A. Antonini, J. Electrochem. Soc. 144 (1997) 1553.
[5] M.M. Thackeray, M.H. Rossouw, R.J. Gummow, D.C. Liles, K. Pearce, A. De Kock, W.I.F. David, S. Hull, Electrochim. Acta 38 (1993) 1259.
[6] A.G. MacDiarmid, J.C. Chiang, A.F. Richter, N.L.D. Somasiri, A.J. Epstein, in: D. Riedel, L. Alcacer (Eds.), Conducting Polymers, Dordrecht, Holland, 1985, 105.
[7] V. Manev, A. Momchilov, A. Kozawa, in: R.J. Brodd (Ed.), Progress in Batteries and Battery Materials, ITE-JEC Press, Japan 14, 1995.
[8] M.R. Rossouw, A. de Kock, D.C. Liles, R.J. Gummow, M.M. Thackeray, J. Mater. Chem. 2 (1992) 1211.
[9] K.S. Hwang, T.H. Yoon, C.W. Lee, Y.S. Son, J.K. Hwang, Journal of Power Sources 75 (1998) 13.
[10] K.M. Abraham, M. Alamgir, J. Electrochem. Soc. 137 (1990) 1657.
[11] M.M. Thackeray, in: R.J. Brodd (Ed.), Progress in Batteries and Battery Materials, ITE-JEC Press, Japan 14, 1995.
[12] S.I. Pyun, J.S. Bae, Electrochim. Acta 41 (1996) 919.
[13] R. Xue, H. Huang, M. Menetrier, L. Chen, Journal of Power Sources 43–44 (1993) 431.
[14] J. Pang, A. Briceno, Chander, J. Electrochem. Soc. 137 (1990) 3447.
[15] C. Barbero, M.C. Miras, R. Kötz, O. Haas, in: N. Doddapaneni, A.R. Landgrebe (Eds.), Lithium Batteries, The Electrochemical Society Proceedings Series, Pennington, NJ PV 94-4, 1994, 281.
[16] A.J. Bard, L.R. Faulkner, Electrohemical Methods; Fundamentals and Applications, Wiley, New York, 1980.